Boosting the Efficiency and Stability of Blue TADF Emitters by Deuteration

Tianyu Huang[1], Dongdong Zhang[1]*, Ge Zhan[2], Qi Wang[1], Guomeng Li[1], Xiangchen Hong[1], Ziyang Liu[1], Lian Duan[1,3]*

[1] Key Laboratory of Organic Optoelectronics, Department of Chemistry, Tsinghua University, Beijing 100084, China

[2] Beijing National Laboratory for Molecular Sciences (BNLMS), State Key Laboratory of Rare Earth Materials Chemistry and Applications, College of Chemistry and Molecular Engineering, Peking University Beijing, 100871, China

[3] Center for Flexible Electronics Technology, Tsinghua University, Beijing 100084, China.

E-mail: ddzhang@mail.tsinghua.edu.cn; duanl@mail.tsinghua.edu.cn

Keywords: deuteration, thermally activated delayed fluorescence, device stability, potential energy surface, blue OLED

Abstract:

Deep-blue organic light-emitting diodes (OLEDs) with both high efficiency and stability remain exclusive in scientific literatures after decades of research. A key reason is the chemical bond dissociation through conical intersections between potential energy surfaces (PESs) of energetically-hot excited states and dissociative states. Here, we report a deuteration strategy to stabilize blue thermally activated delayed fluorescence (TADF) emitters. It is unveiled that deuteration would lower high-frequency vibrations to create shallower PESs in both ground and excited states, energetically retarding the cross of the conical intersection point in dissociative process and alleviate vibrational coupling to eliminate nonradiative decay. With a deuterated blue TADF compound, namely 2,3,4,5,6-pentakis(9H-carbazol-9-yl-*d*8) benzonitrile, as the sensitizer, a deep-blue OLED simultaneously achieves a peak external quantum efficiency of 30.3%, a Commission Internationale de L'Eclairage (CIE) coordinate y value of 0.17, and a superb LT80 (time to 80% of initial luminance) of 227 h at 1000 cd/m^2. And a blue OLED with a CIE_y~0.19 shows an even longer LT80 of 456 h at 1000 cd/m^2.

Introduction

Being one of the three primary colors, blue is indispensable for displays and lightings. However, efficient and stable blue organic emitters for organic light-emitting diodes (OLEDs) have puzzled the researchers for decades. As an OLED ages during continuous operation, a small portion of its molecules will chemically degrade over time to form defect sites, which then act as luminance quenchers, nonradioactive recombination centers and deep charge traps, finally arousing the luminance loss.[1] The formation of defects has been convincingly assigned to the annihilation between bimolecular excited states, finally giving birth to an energetically-hot excited states to dissociate molecule bonds. The spin-allowed symmetric singlet excitons (S_1) feature rapid radiatively decay process to compete the annihilations and thus fluorophores that can only harness S_1 exhibit high stability but low efficiency.[2,3] Conceptually advanced emitters, including noble-metal-based organometallic phosphors[4,5] and thermally activated delayed fluorophores (TADF),[6-8] have been developed to recycle the spin-forbidden unsymmetric triplet excitons. The long-lived triplets, however, are more likely to participate into the annihilation progress.[9] Thus, though ultimate high device efficiency, phosphorescent and TADF OLEDs always suffer from worse stability than fluorophores, particularly in the blue region.

This invokes a new issue, that is, if the lifetime of blue devices that take fully use of the triplet excitons can be promoted? Principally, the most straightforward way is to reduce the triplet concentration and/or shorten its lifetimes. With this in minds, progresses have been made in sky-blue OLEDs. Forrest and co-workers successfully achieved tenfold increase in the lifetime

of sky-blue phosphorescent OLEDs utilizing a graded-dopant-concentration profile to lower triplet concentrations.[10] And later by introducing a manager to quickly consume the hot excited states, the device stability was further improved up to LT80 (LT*x* means time to *x*% of initial luminance) of 334 h but only moderate external quantum efficiency (EQE) of ~9% and a Commission Internationale de L'Eclairage coordinate y value (CIE_y) of 0.31 at 1000 cd/m^2. As for TADF OLEDs, a fast reverse intersystem crossing (RISC) process is believed to be effective in consuming excited states to avoid annihilations. This goal can be fulfilled by introducing hetero-donors to enhance the mixing of excited states with different nature, realizing superb LT97 of 110 h with CIE_y of 0.44 and EQE of 20.8% at 1000 cd/m^2.[11] Cui *et al.* also developed sky-blue TADF emitters with multiple donor units to enlarger spin-orbit couplings and realized a large RISC rate (k_{RISC}) of ~10^7 s^{-1}, accounting for a long LT90 of ~600 h, an EQE of 28.6% at 1000 cd/m^2 and an emission peak at 486 nm, respectively.[12]

Albeit these progress, deep blue devices with CIE_y<0.2, however, still lag behind the sky-blue ones. The difficulty arises from the fact that the energy of hot excited-states can be extremely high in deep-blue emitting systems and thus being more conspicuous to deteriorate the device stability. To circumvent this issue, a sensitized fluorescence emission mechanism has been proposed with blue phosphors or TADF materials as sensitizers to assist triplet harvest for stable fluorescent dopants through Förster energy transfer (FET) process. The long-range FET interaction with extremely high rates of 10^8-10^{11} s^{-1} enables quick consumption of triplet excitons to suppress triplet-related annihilations and improve device stability.[13] Recently,

multiple resonance (MR) fluorescent emitters with narrow bandwidth emission have been adopted as the final emitters, offering a purer emission color with relatively lower excited state energy. Deep blue Ir(III) and Pt(II) phosphors have been adopted as sensitizer for a well-known MR emitter, N7,N7,N13,N13,5,9,11,15-octaphenyl-5,9,11,15-tetrahydro-5,9,11,15-tetraaza-19b,20bdiboradinaphtho[3,2,1-de:1′,2′,3′-jk]pent-acene-7,13-diamine (*ν*-DABNA), realizing extended LT50s of 121 h (CIE_y of 0.162, EQE of 23.3%) and 156.1 h (CIE_y of 0.141, EQE of 25.4%) at an initial luminance of 1000 cd/m^2, respectively.[14,15] By using *ν*-DABNA as the final emitter, TADF-sensitized-fluorescence (TSF) OLEDs achieved LT50 of 151 h (CIE_y of 0.17, EQE of 25.2%) and LT95 of 11 h (CIE_y of 0.20, EQE of 20%) respectively also at an initial luminance of 1000 cd/m^2, comparable or even better than the phosphor sensitized ones.[16,17] Those preliminary works testify the viability of TSF in breaking the efficiency-stability limitation of deep-blue OLEDs with metal-free all purely organic molecules, which, however, still requires the development more stable blue TADF sensitizers.

Deuteration had been reported to be an effective way to improve the stability of conventional fluorescent, phosphorescent emitters and host materials as well.[18-21] However, deuteration effect on TADF emitters remain unexplored and the underlying mechanism is not clear. Herein, we studied deuterated blue TADF emitters with the aim to improve the efficiency and stability. It is revealed that deuteration can lower the energy of vibrational levels establish shallow potential energy surface (PES) by in both ground and excited states. This shallow PES hinders the cross of

the conical intersections between the PESs of the hot excited states and the dissociative states and thus suppress molecular dissociation. Also, vibrational coupling via high-energy vibration levels can be alleviated, thus eliminating nonradiative decay. The proof-of-the-concept deuterated blue TADF emitter exhibited both improved electroluminescence stability and efficiency compared with the undeuterated one. And with this deuterated blue TADF compounds as sensitizers, deep-blue OLEDs simultaneously displayed a maximum EQE of 30.3%, a CIE_y value of 0.17, a full-width at half-maximum (FWHM) of 27 nm and a superb LT80 of 227 h at an initial luminance of 1,000 cd/m^2. Using a redshifted final emitter with a FWHM of only 19 nm, blue device with CIE_y of 0.19 can even realize a LT80 of over 450 h at an initial luminance of 1,000 cd/m^2. This work may shed new light on the development of highly efficient and stable deep-blue emitters.

Results

Molecular design and theoretical analysis

Fig. 1a shows the Jablonski diagram of the possible relaxation pathways for excitons. The hot state can be either an exciton or polaron state resulting from either exciton-exciton annihilation or exciton-polaron annihilation, respectively. While most hot states rapidly relax to the lowest excited states, those that have sufficient higher energy than the dissociative states can lead to the chemical bond dissociation. Technically, this dissociation process happens at the conical intersection point between PESs of hot singlet/triplet excited states (S_n*/ T_n*) and dissociative states. Therefore, the energy of S_n*/ T_n* should reach the conical intersection point to induce

bond dissociation. Besides the electronic energy level, vibrational energy levels also matter in this process, though having been neglected in previous reports. Emitters with high vibrational energy levels, that have relatively deep PESs, are more susceptible to reach the energy point of conical intersection and induce dissociation process. Alternatively, if the S_n*/ T_n* states possess shallow PESs, *i.e.*, low vibration energy levels, the chances to reach the energy crossing point of conical intersection of dissociation process may, theoretically, be significantly reduced and thus suppressing the possibility of bond dissociation. Besides a good long-term stability, a high efficiency is equally important for TADF emitters. The vibrational coupling between high energy vibration levels of the ground state (S_0) and the low energy vibration level of S_1/T_1 has been convincingly recognized as main reason for nonradiative decay. It is reasonable to expect that a shallow PES should also favor to alleviate vibrational coupling to eliminate nonradiative decay.

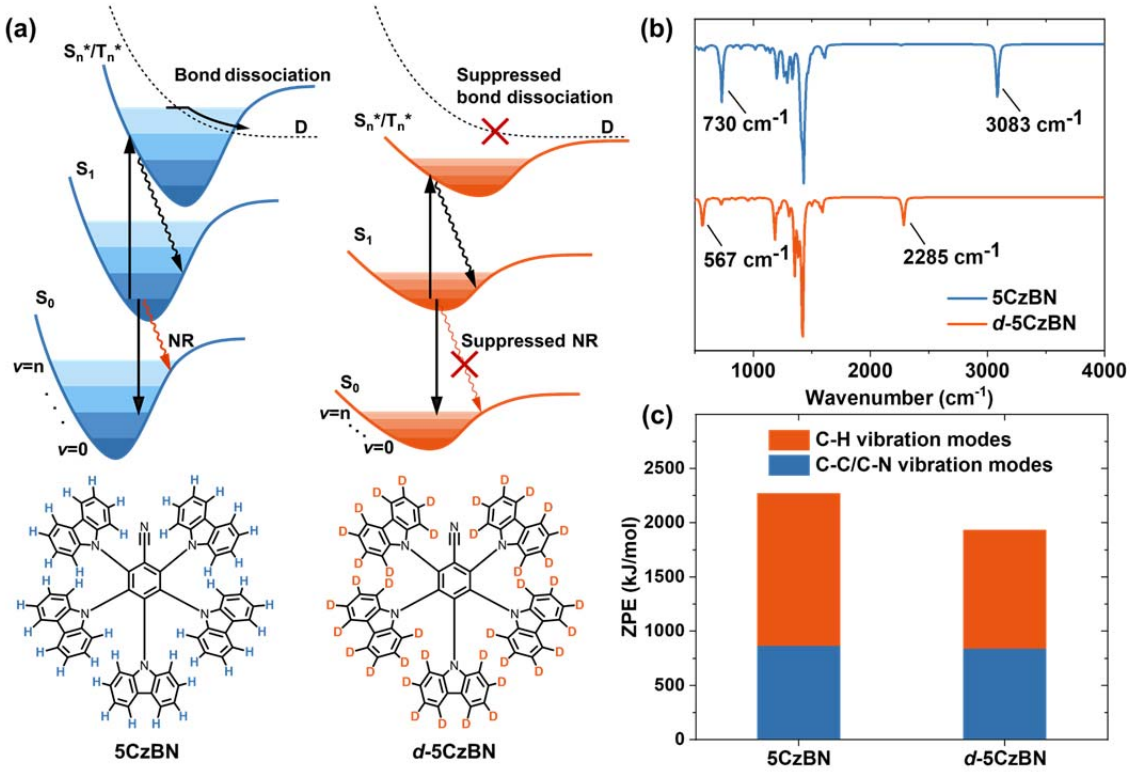

Figure 1 (a) Jablonski diagram of the possible relaxation pathways for excitons and chemical structures of 5CzBN and *d*-5CzBN. (b) Simulated FT-IR spectra of 5CzBN and *d*-5CzBN. (c) Contributions of different vibration modes to molecular ZPE of 5CzBN and *d*-5CzBN.

In the aromatic light-emitting π-systems, high frequency vibration usually originates from C-H stretching and bending. Previous kinetic isotope effect has revealed that replacing hydrogen atom with deuterium (D) can significantly alleviate those high frequency vibrations.[22] Therefore, based on the above discussion, deuterated TADF emitters possess the potential to achieve superior stability and high efficiency simultaneously. To validate this idea, 2,3,4,5,6-penta(9H-carbazol-9-yl) benzonitrile (**5CzBN)** was chosen as a template molecule. This multiple-donors compound is one of the widely studied sky-blue TADF emitters.[23] By replacing carbazole (Cz) units with deuterated carbazole, we synthesized the deuterated analog of 5CzBN, namely ***d*-5CzBN**. To elaborate the isotope effect of *d*-5CzBN, we first carried out

theoretical calculations. Commonly, quantum chemistry programs are designed based on Born-Oppenheimer approximation, which means the mass of nucleus is not taken into account for the electron structure calculation. In other words, the electronic behaviors including excitation states are not bothered by deuterium effect in theoretical calculation. As a result, the calculated electronic transition properties for both 5CzBN and *d*-5CzBN are the same and we will verify that the two molecules do exhibit identical S_1 and T_1 energy state in the following content. However, the results of frequency analysis and thermodynamics are affected by isotope setting since the calculations are based on mass-weighted coordinate system. **Fig. 1b** displays the simulated FT-IR spectrum of both emitters, clearly revealing that the highest energy of observed absorption band for C-H stretching modes is shifted from ~3083 to ~2285 cm^{-1} and C-H bending modes shifted from ~730 cm^{-1} to ~567 cm^{-1} after deuteration. The same phenomenon was also recorded from the experimental result shown in **Supplementary Fig. 1**, evidencing that deuteration could effectively suppress the high frequency vibrations of molecules. Also, it is interesting to note that, for other low frequency vibration, deuteration exhibits quite limited influence. Other evidence that proves the alleviated high frequency vibrations should be the zero-point energy (ZPE) value of those two compounds. It is found that replacing proton with deuterium can significantly reduce the ZPE of the molecule. And the contribution of different normal vibration modes to ZPE of the molecules was analyzed by Shermo program as shown in **Fig. 1c**.[24] The vibrations from aromatic skeleton including carbon-carbon (C-C) and carbon-nitrogen (C-N) bonds contribute similar ZPE value before and after deuteration and the

decreased ZPE value from 5CzBN to *d*-5CzBN mainly originate from the lower frequency vibrations of C-D than C-H. Based on those evidence, it can be concluded that compared with 5CzBN, *d*-5CzBN should possess relatively shallower PES since its high frequency vibrations are suppressed, which is exactly the aim of this molecular design strategy.

Material characterization

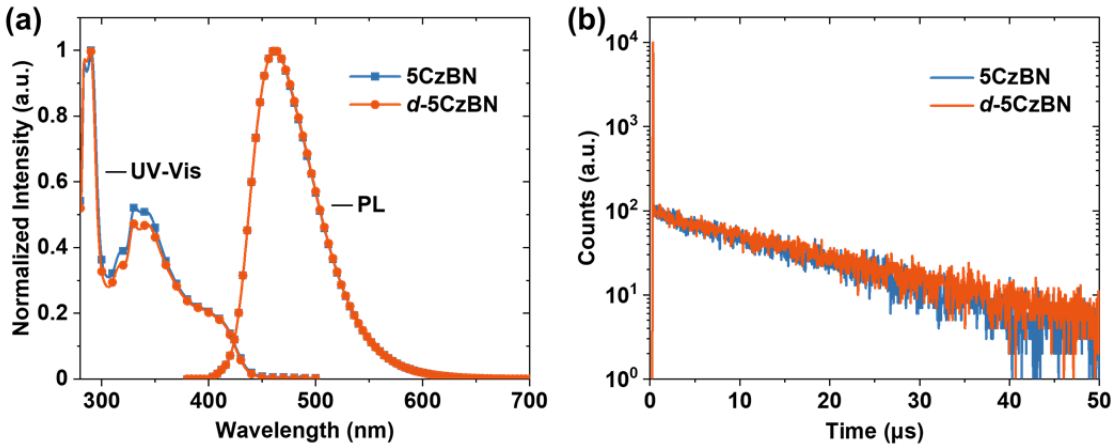

Figure 2 (a) Absorption and PL spectra of 5CzBN and *d*-5CzBN in toluene solution (10^{-5} mol L^{-1}). (b) Transient PL spectra of 5CzBN and *d*-5CzBN in toluene solution (10^{-5} mol L^{-1}).

Table 1 Photophysical properties of *d*-5CzBN and 5CzBN.

	S_1 [a] (eV)	T_1 [a] (eV)	HOMO [b] (eV)	LUMO [c] (eV)	τ_p [d]	τ_d [d]	Φ_{PL} [d]	k_r ($\times10^7$ s^{-1})	k_{ISC} ($\times10^8$ s^{-1})	k_{RISC} ($\times10^5$ s^{-1})	k_{nr}^T ($\times10^4$ s^{-1})
***d*-5CzBN**	2.91	2.66	5.49	2.66	5.3	11.4	0.95	2.26	1.66	6.89	0.50
5CzBN	2.91	2.66	5.48	2.65	4.9	9.9	0.78	2.24	1.82	6.81	2.61

[a] Measured in the toluene solution with a concentration of 10^{-5} mol/L. [b] Calculated by LUMO and energy gap measured by UV-vis. [c] Measured in dry N, N-dimethylformamide with a concentration of 10^{-3} mol/L. [d] Measured in the N_2-saturated toluene solution with a concentration of 10^{-5} mol/L.

To further uncover the effect of deuteration, electrochemical and photophysical properties of 5CzBN and *d*-5CzBN are compared in detail. As shown in **Supplementary Fig. 2**, LUMO energy levels of 5CzBN and *d*-5CzBN were estimated by cyclic voltammetry, being -5.49 and

-5.48 eV, respectively. Also, identical optical energy gaps can be obtained for both emitters (2.83 eV) from their ultraviolet-visible (UV-vis) absorption spectra measured in toluene (10^{-5} mol L^{-1}) as shown in **Fig. 2a**. HOMO energy levels of -2.66 eV for 5CzBN and -2.65 eV for *d*-5CzBN thereof can be obtained. The almost same energy level of frontier molecular orbitals indicate that deuterium substitution has nearly no influence on electron configuration.

Interestingly, identical photoluminescence (PL) fluorescent and phosphorescent spectra were recorded at room temperature and 77K of 5CzBN/*d*-5CzBN in toluene solution as illustrated in **Fig. 2a** and **Supplementary Fig. 3**, respectively. The S_1 and T_1 energies of 5CzBN and *d*-5CzBN were measured to be exactly the same from the onset and the peak wavelengths, being 2.91 and 2.66 eV, respectively. Those performances suggest that deuteration does not affect the radiative decay energy levels. This is understandable that the radiative decay energy levels are mainly determined by the relatively low vibration energy levels, which were not influenced by the deuteration as proved above. Actually, the maintained PL spectra has been widely observed for deuterated organic compounds.[18]

On the contrary, a photoluminescence quantum yield (PLQY) of 0.95 was obtained for *d*-5CzBN in the degassed solution while only 0.78 was recorded for 5CzBN. This suggests the significantly suppressed nonradiative decay process in *d*-5CzBN. The PL decay curves in the solution was also recorded, revealing a prompt/delayed lifetime of 5.3 ns/11.4 μs and 4.9 ns/9.9 μs for *d*-5CzBN and 5CzBN, respectively. The TADF dynamic processes, involving rates of S_1 radiative decay, intersystem crossing, reverse intersystem crossing and T_1 nonradiative decay,

193 have been calculated and listed in **Table 1**. Interestingly, k_r and k_{RISC} are quite similar for both
194 emitters, suggesting that the deuteration would not influence the radiative decay and RISC
195 processes. On the contrary, only a one-fifth k_{nr}^{T} was observed for *d*-5CzBN compared with
196 5CzBN, evidencing that deuteration favors to suppress the nonradiative decay of T_1.
197 Unfortunately, the present calculation method cannot distinguish nonradiative decay and ISC
198 process from S_1.[9] Therefore, the calculated k_{ISC} utilizing the commonly adopted method should
199 involves both nonradiative decay rate of S_1 (k_{nr}^{S}) and ISC rate (k_{ISC}^{S}). The influence of external
200 factors on ISC and RISC are usually similar, and it is reasonable to assume that k_{ISC}^{S} is also not
201 influenced by deuteration. Therefore, the different in k_{ISC} should originates from the different k_{nr}^{S}
202 of both emitters. And it is clear that k_{nr}^{S} in 5CzBN is more significant than that of *d*-5CzBN.
203 Therefore, deuteration should suppress nonradiative decay process of both S_1 and T_1, giving birth
204 to both longer τ_p and τ_d as well as relatively higher PLQY of *d*-5CzBN. Those results herein
205 validate our inspirations that deuteration induced shallow PES favors suppressed nonradiative
206 decay.
207 The photophysical properties of the two emitters were also compared in doped films with a host
208 material named 9-(3-(9H-carbazol-9-yl)phenyl)-9H-3,9'-bicarbazole (mCPBC). As exhibited in
209 **Supplementary Fig.4**, with the increasing doping concentration in mCPBC, both emitters
210 showed red-shifted emission peak. Interestingly, *d*-5CzBN film exhibited an increased FWHM
211 than that of 5CzBN film. This phenomenon can be attributed to the difference in molecular
212 interaction that leads to different conformations of *d*-5CzBN and 5CzBN in solid film. As a

reference, single crystals of *d*-5CzBN and 5CzBN were prepared and analyzed. With the structures shown in **Supplementary Fig. 6**, *d*-5CzBN exhibits smaller dihedral angles between Cz units and central benzene ring compared with 5CzBN. And the difference we believe should arise from the different volume of H and D atom.[25] The S_1 energy of *d*-5CzBN and 5CzBN based on their crystal structure have been calculated by TDDFT calculation, exhibiting higher energy values for *d*-5CzBN (**Supplementary Table 1**). The topologies of the molecular packing are also different from each other (**Supplementary Fig. 7**). Thus, it is understandable that the different molecular interaction should accounts for the different of PL spectra in doped films. The PL decay curves of the doped films were also measured, displaying relatively longer prompt and delayed lifetimes of *d*-5CzBN than 5CzBN (**Supplementary Fig. 5**). Combining with the higher PLQY of *d*-5CzBN, the different in exciton lifetimes should also be attributed to the significantly suppressed nonradiative decay process in *d*-5CzBN, which is in agreement with the results obtained from the solution.

Device performance

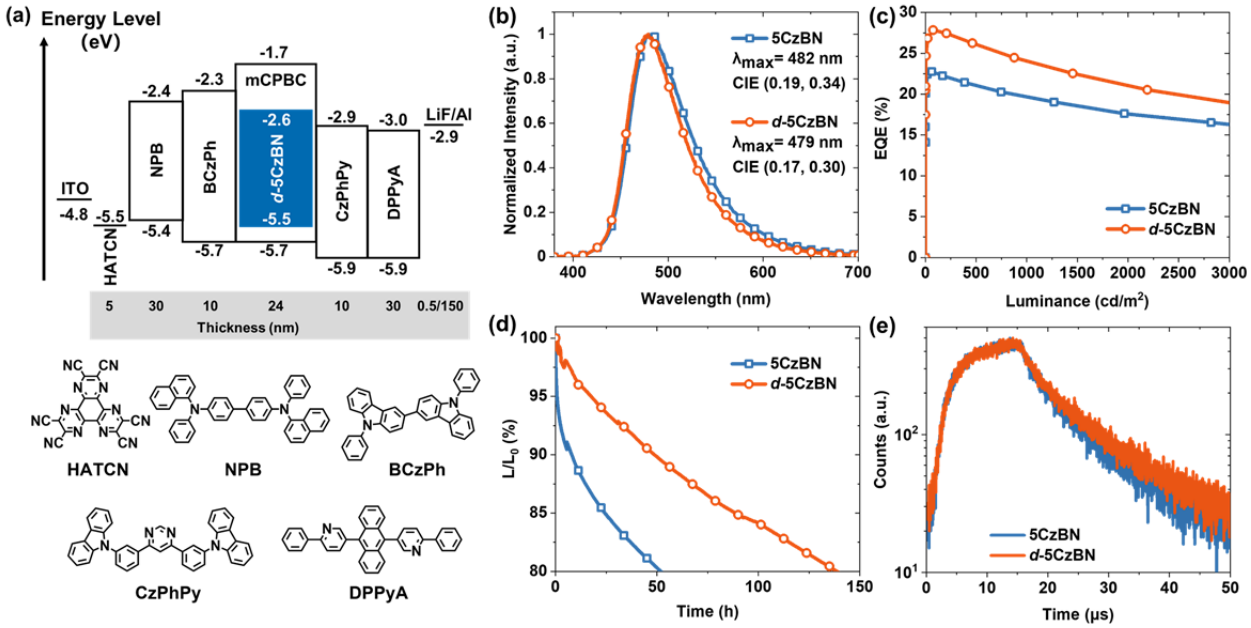

Figure 3 (a) Device configuration and molecular structures of the materials used in devices. (b) EQE vs. luminance characters of devices. (c) EL spectra of devices. (d) Lifetime of devices (at an initial luminance of 1000 cd m^{-2}). (e) EL transient spectra of devices.

The electroluminance (EL) performances of 5CzBN and *d*-5CzBN were compared with device structures of ITO/ HATCN(5 nm)/ NPB(30 nm)/ BCzPh(10 nm)/ mCPBC: 20 wt% emitter (24 nm)/ CzPhPy (10 nm)/ DPPyA (30 nm)/ LiF (0.5 nm)/ Al (150 nm). **Fig. 3a** provides the energy levels and chemical structures of the materials adopted in the device while **Fig. 3b** exhibits the EL spectra with both emission peaks around 480 nm. Also, similar to the PL spectra of doped films, a relatively narrow emission band was obtained for *d*-5CzBN. Consequently, a relatively bluer CIE coordinate of (0.17, 0.30) was recorded for *d*-5CzBN based device and (0.19, 0.34) for device with 5CzBN. The EQE-luminance characters were provided in **Fig. 3c**, exhibiting a high maximum EQE of 27.8% for *d*-5CzBN device while a moderate EQE_{max} of 22.7% for 5CzBN device. The relatively higher device efficiency of *d*-5CzBN naturally should be assigned to its

higher PLQY. Also, a relatively low efficiency roll-off was observed for *d*-5CzBN device with EQE remain 24.2% under luminance of 1000 cd/m^2. A power efficiency as high as 57 lm/W was also obtained for *d*-5CzBN, higher than that of 5CzBN device (53 lm/W).

The operational stabilities of the two devices were also measured at an initial luminance of 1000 cd m^{-2}, of which the results were provided in **Fig. 3d**. A LT80 of 140 h was recorded for *d*-5CzBN device, which is almost 3-times longer than the 5CzBN-based device (LT80 = 53 h). To reveal the origin of the significantly improved device efficiency and stability, the EL transient decay curves of the two devices were illustrated in **Fig. 3e**. Similar to PL transient decay curve in mCPBC film, device based on 5CzBN shows a faster decay which means that the device suffers more from non-radiative decay process than *d*-5CzBN device. More importantly, although relatively long exciton lifetime of *d*-5CzBN device, which should induce more significant exciton annihilations for energetically hot excited states, the 3-fold increasement in LT80 suggests the good endurance of *d*-5CzBN under excited states, which should arise from shallow PES as aforementioned. Those results validate our inspiration that deuteration induced shallow PES favors high stability under excitation.

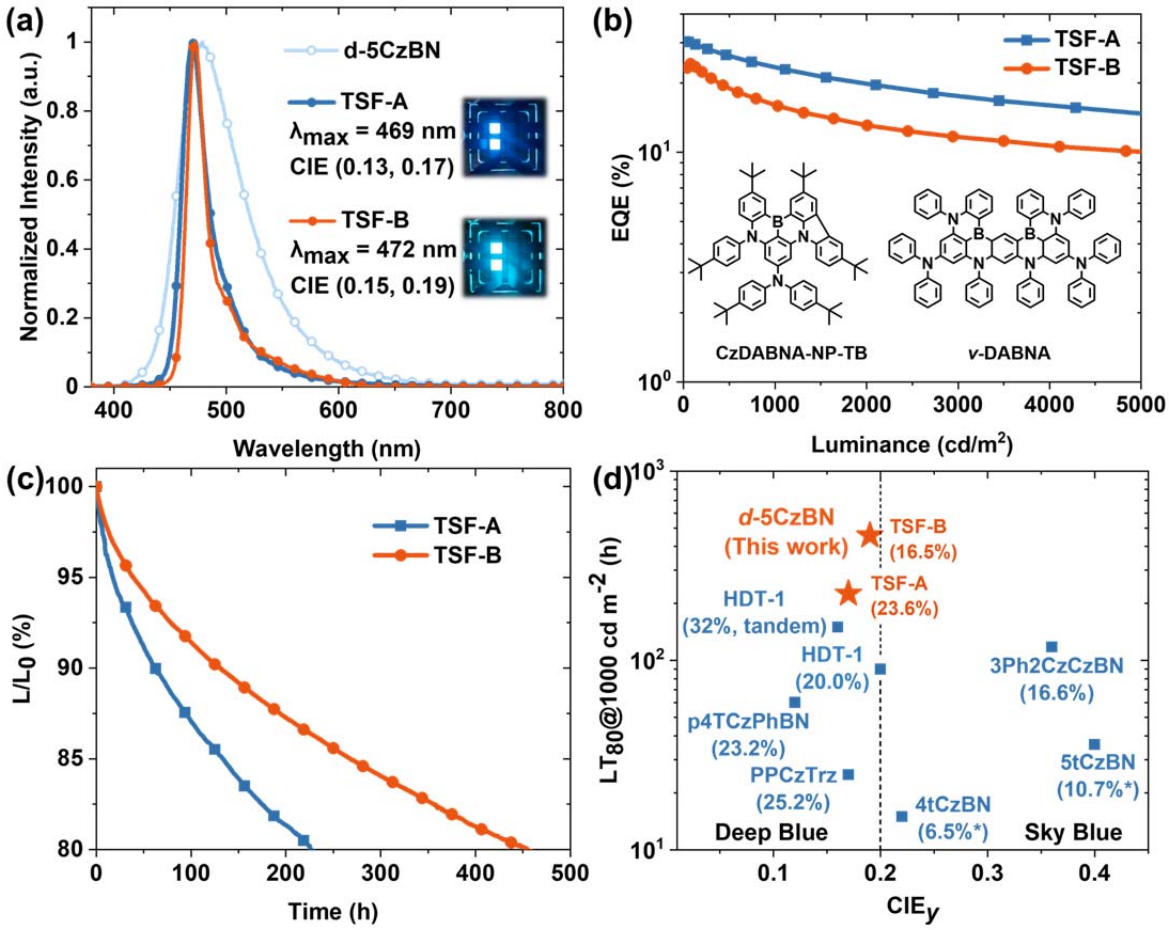

Figure 4 (a) EL spectra of the TSF-A, TSF-B and *d*-5CzBN devices; (b) EQE vs. luminance characters of the TSF-A and TSF-B device. (Inset: molecular structure of CzDABNA-NP-TB and ν-DABNA). (c) Lifetime of the TSF-A and TSF-B device (at an initial luminance of 1000 cd m^{-2}). (d) A comparison of device lifetime with different CIE_y values for stable blue TADF OLEDs. EQE at 1000 cd m^{-2} were labeled in the parenthesis. (*EQE at 500 cd m^{-2})

Though the significantly improved device lifetimes, *d*-5CzBN based devices only showed sky-blue emission. Strategy to realize deep blue devices is utilizing *d*-5CzBN as a TADF sensitizer while introducing an emitter with a narrowband emission. Here, a previously reported MR-TADF dopant, CzDABNA-NP-TB, was adopted as the deep blue emitter.[26] As illustrated in **Supplementary Fig.10**, this compound shows a narrow band emission peaked at 464 nm with a

FWHM of 21 nm and a PLQY of ~100% in toluene solution (10^{-5} mol L^{-1}) and a narrow sharp absorption peak at 450 nm was also observed. Owing to this small stokes shift, a significant spectra overlap between the wide emission spectrum of sensitizer and the absorption spectrum of dopant can be observed, giving birth to a large radii of FET of 3.62 nm. Efficient energy transfer thereby can be expected from sky-blue TADF sensitizer to deep-blue narrowband emitter. The structure of this TADF-sensitized fluorescent device (TSF-A) was ITO/ HATCN (5 nm)/ NPB (30 nm)/ BCzPh (10 nm)/ mCPBC: 20 wt% *d*-5CzBN: 1 wt% CzDABNA-NP-TB (24 nm)/ CzPhPy (10 nm)/ DPPyA (30 nm)/ LiF (0.5 nm)/ Al (150 nm).

Table 1 Summary of device performances

Device	λ_{EL} (nm)	V_{on} (V)	EQE (%)		Power Efficiency (lm/W)		FWHM (nm)	CIE (x, y)	LT80[a)] (h)
			Max	1000 cd/m^2	Max	1000 cd/m^2			
5CzBN	482	2.8	22.7	19.5	53.1	34.2	72	0.19, 0.34	53
d-5CzBN	479	2.8	27.8	24.2	57.3	38.6	69	0.17, 0.30	140
TSF-A	469	2.8	30.3	23.5	50.9	24.1	26	0.13, 0.17	227
TSF-B	472	2.6	24.3	16.5	35.1	16.6	19	0.15,0.19	456

[a)] Recorded at an initial luminance of 1000 cd m^{-2}.

The EL spectra of the TSF devices were shown in **Fig. 4a**, showing strong emission from dopant. Interestingly, owing to the extremely small FWHM of 26 nm, a deep-blue emission with CIE coordinate of (0.13, 0.17) was observed, even though the emission peak is located at a relatively long wavelength of 469 nm. This evidence the advantages of narrow band emitter to obtain deep-blue emission. **Fig. 4b** showed the EQE-luminance characters of the TSF devices,

exhibiting a remarkable EQE_{max} of 30.3% which remains 23.5% at practical brightness of 1000 cd m^{-2}. The EQE_{max} significantly outperforms that of the device with *d*-5CzBN as emitter. Besides the fully exciton utilization assisted by sensitizer, the high EQE value can be assigned to the enhanced light outcoupling efficiency benefiting from the preferred horizontal orientation of dopant due to its planar structure.[27] Also, a high maximum power efficiency of 50.9 lm/W was obtained. Both the EQE and power efficiency represent one of the highest values among all reported results with similar colors.

The device stability was further testified at an initial luminance of 1000 cd m^{-2} as illustrated in **Fig. 4c**. Remarkably, a superb LT80 of 227 h was obtained. Detailed device data are shown in **Table 2**. Interestingly, compared with device directly utilizing *d*-5CzBN as emitter, the TSF device showed even longer lifetime with blue-shifted emission. This is reasonable given the fact that the emitter with narrow band though exhibits bluer emission possesses even lower exciton energy, defined by the onset energy of fluorescent spectra. Also, the potentially accelerated exciton consumption arising from the rapid radiative decay process of CzDABNA-NP-TB also favors longer lifetimes.

Furthermore, we also adopted a well-known MR dopant, *v*-DABNA, as a final emitter to enhance device stability.[28] Featuring extremely narrow bandwidth, *v*-DABNA has exhibited good long-term stability in devices based on TSF. Device named TSF-B was fabricated with the same device architecture above. The EL spectrum showed an emission peak at 472 nm with a small FWHM of only 19 nm, corresponding to a CIE_y of 0.19. Though a relatively lower EQE_{max}

of 24.3%, a significantly extended long LT80 of 456 h was observed at an initial luminance of 1,000 cd/m^2, which also represents the longest lifetime under this specific color. We summarized recent reported stable bottom emission blue devices with $CIE_y < 0.4$ in **Fig. 4d**.[16,17,23,29,30] Clearly, our results here present a significant improvement in device lifetime, together with the state-of-the-art device efficiency, validating our deuteration strategy to stablilize blue compounds. It is anticipated that by optimizing host materials and device structures such as top-emitting devices, both efficiency and stability can be further improved accompined by even blue-shifted emission.

Discussion

Highly efficient and stable deep-blue OLEDs have continuously been an obstacle for further development of this technology and still face formidable challenges until now. The emergence of TADF emitters have provided a viable alternation for this goal. Finding strategies that can improve stability of TADF emitters have been an exigent task and highly desired in the industry and academia. The deuteration strategy proposed here can simultaneously enhance efficiency and operational stability of blue TADF emitters. From the perspective of both theoretical calculation and experiments, it is confirmed that deuteration can significantly slow down high-frequency vibrations and create a relatively shallow PES in both ground and excited states, energetically favoring to suppress dissociative process and eliminating nonradiative decay. The proof-of-the-concept deuterated blue TADF emitter *d*-5CzBN realized nearly 3-times longer device lifetime with ~1.3 times higher EQE_{max} than the undeuterated one. And the TSF device

with *d*-5CzBN as sensitizer while a narrowband dopant as final emitter, a deep-blue device realized a superb long LT80 of 225 h and extremely high EQE_{max} of 30.3% simultaneously at a CIE_y of 0.17. By further optimizing the final emitter, blue device with CIE_y of 0.19 can even realize a LT80 of 456 h at an initial luminance of 1,000 cd/m^2. Quite recently, Bae *et al*. revealed that deuterating the vulnerable benzylic C-H bond can greatly increase the operational lifetime of phosphors by hampering the possible C-H bond cleavage.[31] And Adachi's group also studied the isotope effect of the host material and found a positive effect on the device stability,[21] which was assigned to the enhanced stable amorphous nature and balanced carrier transport properties. The mechanism disclosed here also works well for previous studies. Our work may pave the way for developing better deep-blue TADF emitters and devices that can rival conventional fluorescent devices.

Methods

General Information. All commercially available reagents were used as received unless otherwise stated. 5CzBN and *d*-5CzBN were synthesized according to Supplementary Information. Mass spectra were recorded on a Shimadzu MALDI-TOF mass spectrometer. The electrochemical measurements were performed with a CHI600E electrochemical workstation by using Pt as the working electrode, platinum wire as the auxiliary electrode, and an Ag wire as the reference electrode standardized against ferrocene/ferrocenium. Organic films for optical measurements were fabricated by thermal evaporation under high vacuum onto clean quartz substrates. UV-vis absorption spectra were recorded by an Agilent 8453 spectrophotometer.

Fluorescence and phosphorescence spectra at steady state were recorded by HITACHI F-7000 Fluorescence Spectrometer. Fluorescence lifetime measurement was carried out with Edinburgh fluorescence spectrometer (FLS1000) using picosecond pulsed diode laser under the excitation at 365 nm. PLQYs were measured by Hamamatsu absolute PL quantum yield spectrometer (C9920-02G) with an integrating sphere.

Theoretical calculation. All theoretical calculations were performed using a density functional theory (DFT) method as implemented in Gaussian 16 and ORCA in gas state.[32,33] Ground-state geometries were optimized by B3LYP functional with the 6-31G(d) basis set. Frequency analysis was performed under the same level with corresponding frequency scale factors.[34] Single point energy was calculated by double hybrid functional B2PLYP-D3 with the def2-TZVP basis set.

Device fabrication and Characterization. Before device fabrication, the ITO glass substrates were precleared carefully. Then the sample was transferred to the deposition system. The devices were prepared in vacuum at a pressure of 5×10^{-6} Torr. The organic layers were thermally evaporated at a rate of 1.0 Å s^{-1}. After the organic film deposition, 0.5 nm of LiF and 150 nm of aluminum were thermally evaporated onto the organic surface. All the organic materials used were purified by a vacuum sublimation approach. The electrical characteristics of the devices were measured with a Keithley 2400 source meter. The electroluminescence spectra and luminance of the devices were obtained on Hamamatsu external quantum efficiency measurement system. All the device fabrication and characterization steps were carried out at room temperature under ambient laboratory conditions.

Acknowledgements

This work was supported by the Guangdong Major Project of Basic and Applied Basic Research (Grant No. 2019B030302009), the National Key Basic Research and Development Program of China (Grant Nos. 2017YFA0204501 and 2020YFA0715000), the National Natural Science Foundation of China (Grant Nos. 51903137 and 61890942), the Young Elite Scientists Sponsorship Program by CAST (Grant No. 2019-2021QNRC) and Foshan Xianhu Laboratory of the Advanced Energy Science and Technology Guangdong Laboratory XHT2020-005. The authors would like to thank Miss JiaoJiao Li and Mr. Feng Hu for their assistance in the single crystal analysis.

Author contributions

Tianyu Huang performed the experiments and prepared the manuscript. Ge Zhan synthesized deuterated materials. Dongdong Zhang and Lian Duan conceived and supervised the research. All authors participated in the discussion on experimental results and revised the manuscript.

Competing interests

The authors declare no competing interests.

Reference

1. Wang, D., Cheng, C., Tsuboi, T. & Zhang, Q. Degradation Mechanisms in Blue Organic Light-Emitting Diodes. *CCS Chem.* **2**, 1278-1296, doi:10.31635/ccschem.020.202000271 (2020).

2. Tang, C. W. & VanSlyke, S. A. Organic electroluminescent diodes. *Appl. Phys. Lett.* **51**, 913-915, doi:10.1063/1.98799 (1987).

388 3. Tang, C. W., VanSlyke, S. A. & Chen, C. H. Electroluminescence of doped organic thin films. *J. Appl. Phys.* **65**,
389 3610-3616, doi:10.1063/1.343409 (1989).
390 4. Baldo, M. A. *et al.* Highly efficient phosphorescent emission from organic electroluminescent devices. *Nature* **395**,
391 151-154, doi:10.1038/25954 (1998).
392 5. Ma, Y., Zhang, H., Shen, J. & Che, C. Electroluminescence from triplet metal—ligand charge-transfer excited
393 state of transition metal complexes. *Synthetic Met.* **94**, 245-248, doi:10.1016/S0379-6779(97)04166-0 (1998).
394 6. Uoyama, H., Goushi, K., Shizu, K., Nomura, H. & Adachi, C. Highly efficient organic light-emitting diodes from
395 delayed fluorescence. *Nature* **492**, 234-238, doi:10.1038/nature11687 (2012).
396 7. Kaji, H. *et al.* Purely organic electroluminescent material realizing 100% conversion from electricity to light. *Nat.*
397 *Commun.* **6**, 8476, doi:10.1038/ncomms9476 (2015).
398 8. Wada, Y., Nakagawa, H., Matsumoto, S., Wakisaka, Y. & Kaji, H. Organic light emitters exhibiting very fast
399 reverse intersystem crossing. *Nat. Photonics* **14**, 643-649, doi:10.1038/s41566-020-0667-0 (2020).
400 9. Masui, K., Nakanotani, H. & Adachi, C. Analysis of exciton annihilation in high-efficiency sky-blue organic
401 light-emitting diodes with thermally activated delayed fluorescence. *Org. Electron.* **14**, 2721-2726,
402 doi:10.1016/j.orgel.2013.07.010 (2013).
403 10. Lee, J. *et al.* Hot excited state management for long-lived blue phosphorescent organic light-emitting diodes. *Nat.*
404 *Commun.* **8**, 15566, doi:10.1038/ncomms15566 (2017).
405 11. Noda, H., Nakanotani, H. & Adachi, C. Excited state engineering for efficient reverse intersystem crossing. *Sci.*
406 *Adv.* **4**, eaao6910, doi:10.1126/sciadv.aao6910 (2018).
407 12. Cui, L.-S. *et al.* Fast spin-flip enables efficient and stable organic electroluminescence from charge-transfer

states. *Nat. Photonics* **14**, 636-642, doi:10.1038/s41566-020-0668-z (2020).

13. Kasha, M. Energy Transfer Mechanisms and the Molecular Exciton Model for Molecular Aggregates. *Radiat. Res.* **20**, 55-70, doi:10.2307/3571331 (1963).

14. Chung, W. J. *et al.* Over 30 000 h Device Lifetime in Deep Blue Organic Light-Emitting Diodes with y Color Coordinate of 0.086 and Current Efficiency of 37.0 cd A−1. *Adv. Opt. Mater.*, 2100203, doi:10.1002/adom.202100203.

15. Nam, S. *et al.* Improved Efficiency and Lifetime of Deep-Blue Hyperfluorescent Organic Light-Emitting Diode using Pt(II) Complex as Phosphorescent Sensitizer. *Adv. Sci.*, 2100586, doi:10.1002/advs.202100586.

16. Chan, C.-Y. *et al.* Stable pure-blue hyperfluorescence organic light-emitting diodes with high-efficiency and narrow emission. *Nat. Photonics* **15**, 203-207, doi:10.1038/s41566-020-00745-z (2021).

17. Jeon, S. O. *et al.* High-efficiency, long-lifetime deep-blue organic light-emitting diodes. *Nat. Photonics* **15**, 208-215, doi:10.1038/s41566-021-00763-5 (2021).

18. Tong, C. C. & Hwang, K. C. Enhancement of OLED Efficiencies and High-Voltage Stabilities of Light-Emitting Materials by Deuteration. *J. Phys. Chem. C* **111**, 3490-3494, doi:10.1021/jp066116k (2007).

19. Abe, T., Miyazawa, A., Konno, H. & Kawanishi, Y. Deuteration isotope effect on nonradiative transition of fac-tris (2-phenylpyridinato) iridium (III) complexes. *Chem. Phys. Lett.* **491**, 199-202, doi:10.1016/j.cplett.2010.03.084 (2010).

20. Wang, P. *et al.* Synthesis of all-deuterated tris(2-phenylpyridine)iridium for highly stable electrophosphorescence: the “deuterium effect”. *J. Mater. Chem. C* **1**, doi:10.1039/c3tc30547c (2013).

21. Liu, X. *et al.* Isotope Effect of Host Material on Device Stability of Thermally Activated Delayed Fluorescence

Organic Light-Emitting Diodes. *Small Sci.*, doi:10.1002/smsc.202000057 (2021).

22. Anslyn, E. & Dougherty, D. A. *Modern Physical Organic Chemistry*. (University Science Books, 2006).

23. Zhang, D. D., Cai, M. H., Zhang, Y. G., Zhang, D. Q. & Duan, L. Sterically shielded blue thermally activated delayed fluorescence emitters with improved efficiency and stability. *Mater. Horiz.* **3**, 145-151, doi:10.1039/c5mh00258c (2016).

24. Lu, T. & Chen, Q. Shermo: A general code for calculating molecular thermodynamic properties. *ChemRxiv*, doi:10.26434/chemrxiv.12278801 (2020).

25. Bartell, L. S. & Roskos, R. R. Isotope Effects on Molar Volume and Surface Tension: Simple Theoretical Model and Experimental Data for Hydrocarbons. *J. Chem. Phys.* **44**, 457-463, doi:10.1063/1.1726709 (1966).

26. Oda, S. *et al.* Carbazole-Based DABNA Analogues as Highly Efficient Thermally Activated Delayed Fluorescence Materials for Narrowband Organic Light-Emitting Diodes. *Angew. Chem. Int. Ed.* **60**, 2882-2886, doi:10.1002/anie.202012891 (2021).

27. Han, S. H., Jeong, J. H., Yoo, J. W. & Lee, J. Y. Ideal blue thermally activated delayed fluorescence emission assisted by a thermally activated delayed fluorescence assistant dopant through a fast reverse intersystem crossing mediated cascade energy transfer process. *J. Mater. Chem. C* **7**, 3082-3089, doi:10.1039/C8TC06575F (2019).

28. Kondo, Y. *et al.* Narrowband deep-blue organic light-emitting diode featuring an organoboron-based emitter. *Nat. Photonics* **13**, 678-682, doi:10.1038/s41566-019-0476-5 (2019).

29. Chan, C.-Y., Tanaka, M., Nakanotani, H. & Adachi, C. Efficient and stable sky-blue delayed fluorescence organic light-emitting diodes with CIEy below 0.4. *Nat. Commun.* **9**, 5036, doi:10.1038/s41467-018-07482-6 (2018).

30. Zhang, D. *et al.* Efficient and Stable Deep-Blue Fluorescent Organic Light-Emitting Diodes Employing a Sensitizer with Fast Triplet Upconversion. *Adv. Mater.* **32**, e1908355, doi:10.1002/adma.201908355 (2020).

31. Bae, H. J. *et al.* Protecting Benzylic C□H Bonds by Deuteration Doubles the Operational Lifetime of Deep-Blue Ir-Phenylimidazole Dopants in Phosphorescent OLEDs. *Adv. Opt. Mater.*, 2100630, doi:10.1002/adom.202100630 (2021).

32. Gaussian 16 Rev. B.01 (Wallingford, CT, 2016).

33. Neese, F. The ORCA program system. *WIRES Comput. Mol. Sci.* **2**, 73-78 (2012).

34. Scott, A. P. & Radom, L. Harmonic Vibrational Frequencies: An Evaluation of Hartree-Fock, Møller-Plesset, Quadratic Configuration Interaction, Density Functional Theory, and Semiempirical Scale Factors. *J. Phys. Chem.* **100**, 16502-16513, doi:10.1021/jp960976r (1996).

Data availability

The data that support the plots within this paper and other findings of this study are available from the corresponding author upon reasonable request.